Dalton Transactions

ROYAL SOCIETY OF CHEMISTRY

PAPER

View Article Online
View Journal | View Issue

Cite this: *Dalton Trans.*, 2025, **54**, 7690

Lone pair electron-induced attrition of lanthanide ions from a sillenite-structured bismuth gallate host†

Nistha Singh,[a,b] Sandeep Nigam, *[a,b] Chiranjib Majumder,[a,b] Nidhi Gupta[c] and Vasanthakumaran Sudarsan*[a,b]

The crucial role of lone pair of electrons in the functionality of materials has been unprecedented. The present study reports a prolific correlation between the local structure and the stereochemical activity of the lone pairs of Bi^{3+} ions in the sillenite structure. The structural changes induced by variations in annealing temperatures greatly influenced the stereochemical activity of Bi^{3+} ion lone pairs, which, in turn, dictated the capacity for the incorporation of probing lanthanide ions in its proximity. Increased annealing temperature induces a transformation of $Bi_{12}GaO_{20\pm\delta}$ samples from a nanoscale to a bulk length scale. During the nano-to-bulk conversion of sillenite-structured $Bi_{12}GaO_{20\pm\delta}$, the emergence of long-range ordering synchronized with the enhanced stereochemical activity of the lone pair, and this amelioration in activity led to the attrition of luminescent lanthanide ions (Eu^{3+}, Tb^{3+}, Er^{3+}, and Yb^{3+}) from the sillenite phase. Based on detailed experimental and theoretical investigations, it was envisioned that while finite size impeded the long-range translational repeatability of lone pairs in the nano-crystalline $Bi_{12}GaO_{20\pm\delta}$ sample, the concurrent existence of random geometrical distortion induces averaging of interactions at the focal Bi-site, suppressing the stereochemical activity. In high-temperature annealed bulk $Bi_{12}GaO_{20\pm\delta}$ sillenite samples, the long-range symmetrical arrangement of Bi^{3+} lone pairs balances the repulsive interactions. To maintain this balance, guest (doped) lanthanide ions were eliminated from the host lattice, resulting in phase separation. It is believed that the observations and rationalizations established between the local structure and the stereochemical activity of Bi^{3+} ion lone pair will aid in designing future bismuth-based functional materials.

Received 17th December 2024,
Accepted 2nd April 2025

DOI: 10.1039/d4dt03483j

rsc.li/dalton

Introduction

Lone pairs play a significant role in determining the geometry, local environment, electronic structure and physicochemical properties of molecules and solids.[1] The effects of lone pairs present in 6th-row p-block elements/ions, such as Tl^{+}, Pb^{2+} and Bi^{3+}, on framework solids/compounds have been extensively investigated for nonlinear optical, photocatalytic and solar energy conversion applications.[2–6] Among the aforementioned ions, Bi^{3+} is the least toxic, and various Bi^{3+}-based compounds are being developed to evaluate their optoelectronic and photocatalytic properties.[2–6] One of the key parameters responsible for the unique properties of Bi^{3+}-based compounds is the extent of stereochemical activity of its lone pair.[1,7] Stereochemically less active or silent lone pairs originate when the $6s^2$ electrons of Bi^{3+} are both spatially and temporally averaged, leading to spherical symmetry.[7] In contrast, when there is a strong interaction between the $6s^2$ electrons of Bi^{3+} and the 2p electrons of oxygen, the lone pair becomes stereochemically highly active.[7–9] It has been demonstrated previously that the interaction of $6s^2$ electrons of Bi^{3+} ions with the 2p orbital of oxide ions leads to unique properties, such as defect tolerance and shallow ionization potentials,[9–12] in bismuth compounds. In addition to the localized 6s → 2p interactions, it has also been reported that the correlated extension of lone pairs over larger length scales in a crystal lattice enhances the stereochemical activity.[1,7] Theoretical reports have demonstrated that the filled antibonding orbital (formed by the interaction of $6s^2$ electrons of Bi^{3+} ions with the 2p orbital of oxygen) interacts with the empty 6p orbital of Bi^{3+} ions. The extent of this interaction (p-orbital mixing) contributes to the enhanced stereochemical activity of the lone pair.[12] The extent

[a]*Chemistry Division, Bhabha Atomic Research Centre, Mumbai 400085, India. E-mail: snigam@barc.gov.in, snigam.jpr@gmail.com*
[b]*Homi Bhabha National Institute (HBNI), Mumbai 400094, India. E-mail: vsudar@barc.gov.in*
[c]*Technical Physics Division, Bhabha Atomic Research Centre, Mumbai 400085, India*
† Electronic supplementary information (ESI) available. See DOI: https://doi.org/10.1039/d4dt03483j

of distortion in the polyhedron around the lone-pair bearing cation also contributes to stereochemical activity.[12] In other words, if the site of the lone pair-bearing cation is spherically isotropic, the lone pair is stereochemically less active. Taking Bi_2YO_4X (X = Cl, Br, I) as an example, Ogawa *et al.*[12] reported that introducing Bi^{3+} ions at the ordered (undistorted) Y^{3+} sites in the lattice leads to high symmetry around the Bi^{3+} environment, resulting in poor stereochemical activity. Thus, long-range ordering of Bi^{3+} and O^{2-} species in the lattice influences the stereochemical activity of the lone pairs.

Rare earth ion luminescence has been widely used to probe the local structure.[13–20] Therefore, it is worth examining the stereochemical activity of Bi^{3+} lone pair by introducing a rare earth ion in its vicinity. In the present study, it is demonstrated for the first time that changes in the luminescence properties of probe species such as Eu^{3+} and Er^{3+} can be used to monitor the conversion of stereochemically silent lone pairs to stereochemically active lone pairs in bismuth-based ternary oxides with a sillenite structure. Sillenite-structured bismuth oxide was chosen in the present study because these compounds contain a large number of five-coordinated Bi^{3+} sites available for substitution, which, in turn provides a significant number of lone pairs and promotes subsequent ordering on larger length scales. Bismuth-based hosts, other than those with a sillenite structure, have been reported earlier for doping with lanthanide ions.[21–25] The host's density of states in the valence band (VB) and conduction band (CB), as well as its position,[21,22] are found to be significantly affected by lanthanide ion doping. Keeping the above in mind, $Bi_{12}GaO_{20\pm\delta}$ samples with nanoscale dimensions were prepared and annealed at different temperatures to convert them into bulk form. During the nano-to-bulk conversion process, the structural changes of all the samples were investigated using a variety of techniques, including, XRD, UV-Visible optical absorption, XPS and photoluminescence. For a deeper insight into temperature-induced structural perturbation, lanthanide ions, such as Eu^{3+}, Yb^{3+}/Er^{3+} and Tb^{3+}, were doped into the lattice, and their luminescence properties were evaluated as a function of annealing temperature. Drastic changes in luminescence properties, including phase segregation of the lanthanide-rich bismuth phase, were observed in the samples annealed at higher temperatures. The increased annealing temperature and associated structural modifications significantly perturbed the stereochemical activity of lone pairs, which in turn affected lanthanide luminescence and led to phase segregation from the sillenite structure. To the best of the authors' knowledge, this type of lone pair-dictated lanthanide luminescence and phase segregation has been reported for the first time.

Experimental details

Materials and methods

Phase-pure $Bi_{12}GaO_{20\pm\delta}$, with and without lanthanide ion doping, was prepared by co-precipitating the precursor ions in an ethylene glycol solution at 150 °C using urea as the precipitating agent. The as-prepared samples were annealed at different temperatures (in an air environment). The inorganic salts used were bismuth nitrate pentahydrate ($Bi(NO_3)_3{\cdot}5H_2O$, M/s SDFine Chem Limited, 98.5%), gallium(III) nitrate hydrate ($Ga(NO_3)_3{\cdot}xH_2O$, formula weight = 255.74 g mol^{-1}, Sisco Research Laboratories Pvt. Ltd, 99.9%) and all lanthanide salts: europium(III) nitrate hydrate ($Eu(NO_3)_3{\cdot}xH_2O$, $x \approx 6$, Alfa Aesar, 99.9%), ytterbium(III) nitrate pentahydrate ($Yb(NO_3)_3{\cdot}5H_2O$, Aldrich, 99.9%), erbium(III) nitrate pentahydrate ($Er(NO_3)_3{\cdot}5H_2O$, Aldrich, 99.9%) and terbium(III) nitrate hexahydrate ($Tb(NO_3)_3{\cdot}6H_2O$, Alfa Aesar, 99.9%). All chemicals were used as received without further purification. Ethylene glycol ($(CH_2OH)_2$), AR grade, was procured from M/s SDFine Chem Limited, Mumbai. Urea ($[CO(NH_2)_2]$, LobaChemie) and ethanol (C_2H_6O) were used as purchased.

Preparation of bismuth gallium mixed oxide ($Bi_{12}GaO_{20\pm\delta}$) sillenites

For the preparation of bismuth gallium mixed oxides, 1205 mg of $Bi(NO_3)_3{\cdot}5H_2O$ (0.209 mmol) was dissolved in 15 mL of ethylene glycol (EG). A stoichiometric amount of $Ga(NO_3)_3{\cdot}xH_2O$ (53 mg, 0.209 mmol) was added to this solution, and the reaction mixture was sonicated at room temperature for 5 min to obtain a clear reaction mixture/solution. The solution was then transferred into a round-bottom flask and subsequently introduced into a silicon oil bath placed over a hot plate to carry out the reaction at a set temperature of 150 °C. Approximately 2 g of urea was added to the reaction medium when the temperature reached about 80 °C. The reaction was continued for 2.5 h. The precipitate was collected by centrifugation, washed thrice with deionized water and once with ethanol, and dried under an IR lamp for one hour, followed by drying for 4h in air to obtain the as-prepared solid powder of bismuth gallium mixed oxides. Subsequently, the as-prepared powder mixture was annealed at 250 °C, 450 °C and 650 °C in silica boats under a static air atmosphere for 4h to produce single-phase $Bi_{12}GaO_{20\pm\delta}$.

Preparation of rare earth doped bismuth gallium mixed oxide ($Bi_{12}GaO_{20\pm\delta}$) sillenites

An aqueous solution obtained by dissolving the required amount of $Eu(NO_3)_3{\cdot}xH_2O$ ($x \approx 6$) (56 mg, 0.209 mmol) was mixed with 15 ml of ethylene glycol medium containing stoichiometric amounts of $Bi(NO_3)_3{\cdot}5H_2O$ (1158.7 mg, 0.209 mmol) and $Ga(NO_3)_3{\cdot}xH_2O$ (53.5 mg, 0.209 mmol). The resulting solution was subjected to sonication in a round-bottom flask for 5 min, after which it was heated to 80 °C in a silicon oil bath. The rest of the procedure was the same as that adopted for the undoped sample to produce single-phase $Bi_{12}GaO_{20\pm\delta}$:5%Eu. A similar procedure was used for preparing Tb^{3+} ($Tb(NO_3)_3{\cdot}6H_2O$, 56.8 mg, 0.209 mmol), Yb^{3+} ($Yb(NO_3)_3{\cdot}5H_2O$, 345.2 mg, 0.356 mmol) and Er^{3+} ($Er(NO_3)_3{\cdot}5H_2O$, 37.9 mg, 0.356 mmol) doped samples, with the exception that stoichiometric amounts of the respective lanthanide ions were used during the reaction.

Results and discussion

Powder X-ray diffraction (XRD) patterns shown in Fig. 1 confirmed that the as-prepared, 250 °C and 350 °C heated samples lacked sufficient crystallinity, whereas the formation of a sillenite-structured bismuth gallate phase ($Bi_{12}GaO_{20\pm\delta}$) was observed for the samples heated at 450 °C and 650 °C (Fig. 1(d and e)). The highly crystalline nature of the 450 °C and 650 °C heated samples was evident from the sharp diffraction peaks observed (Fig. 1(d and e)). Sillenite phases crystallized in a cubic structure (space group *I*23), and based on Rietveld refinement of the XRD patterns, the lattice parameters for the 450 °C and 650 °C heated samples were evaluated and found to be nearly identical (10.193 Å). TEM studies carried out on the samples confirmed that the as-prepared and 250 °C heated samples were nanocrystalline bismuth gallate with a sillenite structure. Representative TEM images and SAED patterns are shown in Fig. S1 of the ESI.† From the XPS studies, the binding energy values corresponding to the $4d_{5/2}$ and $4d_{3/2}$ levels of Bi^{3+} in the as-prepared and heated samples were evaluated and presented in Table S1.† Representative patterns are shown in Fig. S2 of the ESI.† The values were found to be around 441.9 eV and 465.6 eV for all the samples, confirming that the bismuth ion existed in the 3+ oxidation state in both the as-prepared and heated samples.[26–28] It was also inferred that there was no significant change in the coordination number around Bi^{3+} ions in these samples. Energy dispersive X-ray (EDX) and X-ray fluorescence analyses were carried out on the samples to evaluate the Bi/Ga ratio. A representative EDX spectrum is shown in Fig. S3 of the ESI.† The spectrum confirmed the presence of Bi and Ga, along with other elements. Based on the intensity of the peaks corresponding to Bi and Ga, the Bi to Ga ratio was evaluated and found to be ~15 for all the samples. From this value and the general stoichiometry of sillenite-structured bismuth gallate reported earlier,[29] it was inferred that the samples heated at 450 °C and 650 °C were non-stoichiometric in nature, with the composition $Bi_{12}Bi_{0.19}Ga_{0.81}O_{19.5}$.

From the results discussed above, it was clear that the as-prepared, 250 °C and 350 °C annealed samples possessed only short-range order, while long-range order occurred in samples heated above 350 °C. Since lone pairs are present in Bi^{3+}, it is of interest to understand how the transition from short- to long-range order affects the relative orientation/alignment of lone pairs across the length scale and the associated electronic environment around Bi^{3+}. It is expected that, depending on the length scale of orientation/alignment of the $6s^2$ lone pair electrons of Bi^{3+}, the local chemical environment around Bi^{3+} will be modified. Such changes in the chemical environment can influence its electronic structure and may lead to variations in the band gap of the material, as well as in the extent of stereochemical activity of the lone pair.[12] It has been reported that the placement of "s" states far from the valence band leads to lone pairs that are relatively less active.[12]

UV-Visible optical absorption is an ideal technique for monitoring such changes. Fig. 2(a) shows the UV-Visible

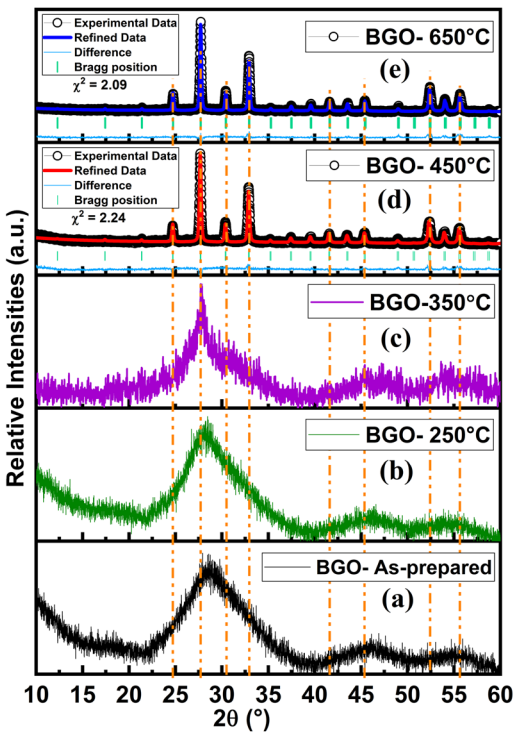

Fig. 1 XRD patterns of (a) as-prepared bismuth gallate (BGO) sample, and those heated at (b) 250 °C, (c) 350 °C, (d) 450 °C and (e) 650 °C. Rietveld refinement was carried out for 450 °C and 650 °C heated samples.

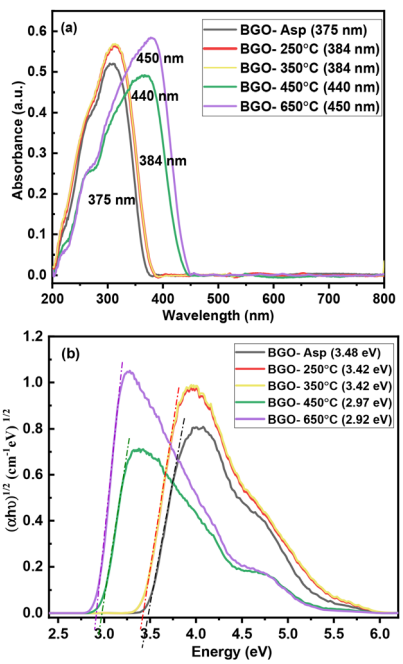

Fig. 2 (a) UV-Visible absorption spectra and (b) plot of $(\alpha h\nu)^{1/2}$ *versus* energy for BGO samples annealed at different temperatures. (All measurements were conducted using the samples in their solid-state form.)

optical absorption spectra for the as-prepared and heated samples. The wavelength corresponding to the onset of absorption for the as-prepared, 250 °C and 350 °C heated samples was found to be in the range of 375–385 nm. Upon heating to higher temperatures (*i.e.* for 450 °C and 650 °C), the onset wavelength shifted to a range of 440–450 nm, as shown in the plot. The optical gap (band gap) was evaluated for these samples based on the method reported by Davis and Mott.[30]

$$\alpha(\nu)h\nu = A(h\nu - E_{opt})^r, \quad (1)$$

where $h\nu$ is the photon energy, "A" is a constant, E_{opt} is the optical gap and "r" represents the nature of the transition process. For an allowed indirect transition, "r" can take the value of 2.

Fig. 2(b) shows the plot of $(\alpha h\nu)^{1/2}$ *versus* $h\nu$ for the samples heated at different temperatures. The energy gap, or band gap, was evaluated by extrapolating the straight-line region of the curve to the x-axis. The value of the energy gap was nearly the same (3.4–3.5 eV) for the as-prepared, 250 °C and 350 °C heated samples. For the high-temperature heated samples, the value decreased to 2.9–3.0 eV. This decrease in the band gap suggested the involvement of lone pair electrons in the bonding. To further understand the changes in electronic structure and the optical/band gap values, theoretical calculations were performed, which are described later in this manuscript.

One way to monitor structural changes occurring in bismuth gallate-based sillenite-structured materials as a function of heat treatment temperatures is to dope the sample with small amounts of lanthanide ions (Er^{3+}, Eu^{3+} and Tb^{3+}) and monitor its luminescence. Since the ionic radius of Bi^{3+} (1.03 Å) under a coordination number of six is comparable to that of Eu^{3+} (0.947 Å), Er^{3+} (0.89 Å), Yb^{3+} (0.868 Å) and Tb^{3+} (0.923 Å)[31] with the same coordination number, it is reasonable to assume that $Eu^{3+}/Tb^{3+}/Er^{3+}/Yb^{3+}$ will replace five-coordinated Bi^{3+} (5 oxygen atoms and 1 lone pair (LP)) in the lattice. It should be noted that the five-coordinated Bi-site in the sillenite-structured bismuth gallate of the present study is slightly different from the conventional five-coordinated sites in inorganic oxides, as it possesses a lone pair of electrons on the central Bi^{3+} species. In other words, Bi^{3+} essentially occupies a pseudo-octahedral site, with five connections to oxygen atoms in the structure and the sixth coordination is with the $6s^2$ lone pair of electrons. Photoluminescence studies have been carried out with the lanthanide ions mentioned above. Representative results are described below.

Fig. 3 shows the emission spectra recorded in the near-infrared (NIR) region for the samples doped with both Yb^{3+} and Er^{3+} ions and heated at different temperatures. All the samples were excited at 980 nm. For the as-prepared sample, a weak and broad emission peak (linewidth ~25 nm) was observed around 1530 nm, which was characteristic of the $^4I_{13/2} \rightarrow {}^4I_{15/2}$ transition of Er^{3+} ions in the host. Upon heat treatment, the linewidth of the emission peak remained the same up to 350 °C, and beyond that, the linewidth decreased.

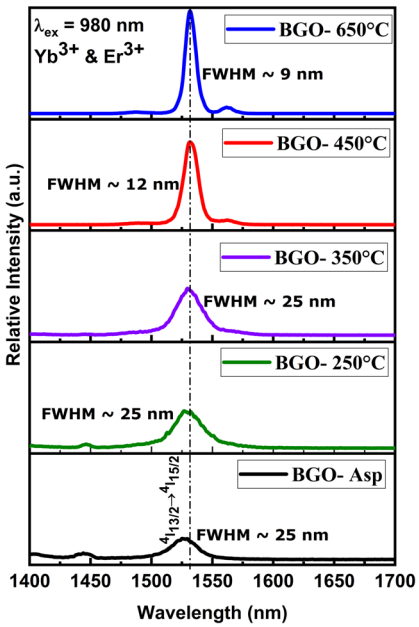

Fig. 3 Emission spectra of BGO samples doped with Yb^{3+} and Er^{3+} ions, heated at different temperatures. All samples were excited at 980 nm.

For the 450 °C and 650 °C heated samples, the linewidths were found to be 12 nm and 9 nm, respectively. The increased linewidths observed for the as-prepared sample and those heated up to 350 °C indicated a distribution in bond lengths and bond angles around Er^{3+} in these samples. In other words, the symmetry around the lanthanide ion improved with increasing temperature. The decrease in the linewidth of the peak (about 50%) suggested that the local environment around Er^{3+} underwent significant ordering for the 450 °C and 650 °C heated samples. XRD studies carried out on the 650 °C heated sample confirmed the formation of a separate phase with the composition $Bi_{0.9}Yb_{0.1}O_{1.5}$. It is worth mentioning that the $Bi_{0.9}Yb_{0.1}O_{1.5}$ compound has a β-Bi_2O_3 structure (ICSD code: 51134),[32] and the corresponding XRD pattern is shown in Fig. S4 of the ESI† (peaks marked "*" represent the $Bi_{0.9}Yb_{0.1}O_{1.5}$ phase). The lattice parameter of the phase-segregated sillenite phase matched well with that of the undoped sillenite phase (10.193 Å), confirming that there was no residual solubility of lanthanide ions in the lattice. A similar trend was also observed in the upconversion luminescence from these samples.

Fig. 4 shows the upconversion emission spectra from Yb^{3+} and Er^{3+} doped as-prepared bismuth gallate samples, along with those heated at different temperatures, namely, 250 °C, 350 °C, 450 °C and 650 °C. Green luminescence, visible to the naked eye, was observed from the as-prepared sample, as shown in the photograph of the emission observed from the sample upon 980 nm excitation (Fig. 4(a) inset). Major peaks observed corresponded to the $^2H_{11/2} \rightarrow {}^4I_{15/2}$ (520 nm), $^4S_{3/2} \rightarrow {}^4I_{15/2}$ (540 nm) and $^4F_{9/2} \rightarrow {}^4I_{15/2}$ (654 nm) transitions of Er^{3+} ions. The relative intensity of the green emission was found to

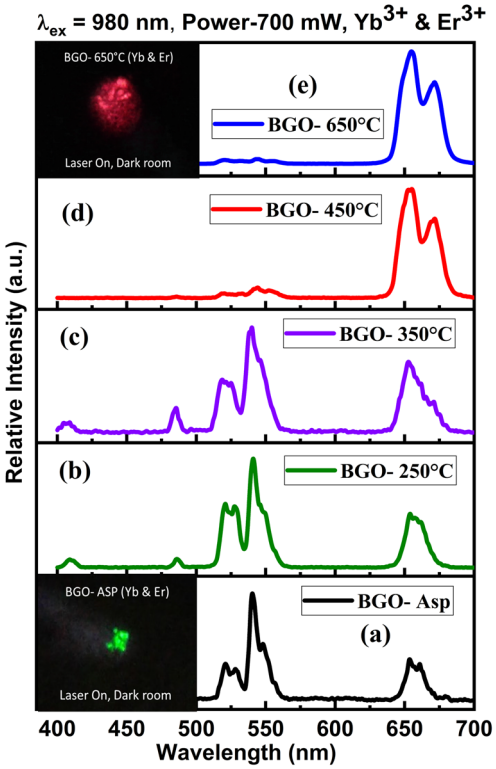

Fig. 4 Upconversion spectra of Yb^{3+}-, Er^{3+}-doped BGO samples heated at different temperatures (a–e). Insets in figures (a) and (e) show photographs of green and red emission from the as-prepared and 650 °C heated BGO samples, respectively.

be higher than that of the red emission from the sample (green to red ratio = 2.5). For the 450 °C and 650 °C heated samples, the intensity of the emission at 654 nm (red emission) was significantly greater than that at 540 nm (green emission) (green to red ratio = 0.05). The intensity of red luminescence increased as the Er^{3+}–Er^{3+} distance decreased in samples heated at higher temperatures (450 °C and 650 °C) due to phase segregation. The enhanced interaction between Er^{3+} ions in the Er^{3+}-enriched segregated phase facilitated more efficient Er^{3+}–Er^{3+} interactions, leading to an increased population in the $^4F_{9/2}$ level of Er^{3+}, which was associated with the increased intensity of the red luminescence. Lee *et al.*[33] reported that decreased Er^{3+} ion spacing enhances cross-relaxation, populating the $^4F_{9/2}$ level and leading to stronger red emission. A photograph of the intense red emission observed from the 650 °C heated sample is shown in the inset of Fig. 4(e).

The relative intensity ratio of green emission (520 nm and 540 nm combined) to red emission (654 nm), known as the green-to-red ratio (GRR), is a parameter that can be used to monitor changes in the environment around Er^{3+} in the lattice. The value was found to be around 2.5 for the as-prepared, 250 °C and 350 °C heated samples. However, for the 450 °C and 650 °C heated samples, the values decreased to 0.05. The drastic decrease in the GRR value confirmed that the Er^{3+} environment was significantly different in the high-temperature heated samples. Based on the XRD pattern of the high-temperature heated sample, as well as control experiments carried out on the Bi_2O_3:Yb,Er system, it was confirmed that the red emission was arising from the phase-separated $Bi_{0.9}Yb_{0.1}O_{1.5}$ phase.[32]

These results were consistent with those obtained from XRD and near-infrared photoluminescence measurements discussed previously. Essentially, lanthanide ions were not retained in the lattice beyond a temperature of 350 °C. In other words, lanthanide ions underwent attrition from the bismuth gallate network at high temperatures.

Finally, both downconversion and upconversion luminescence results obtained from Er^{3+}-doped samples were further substantiated by the photoluminescence studies carried out on Eu^{3+}- and Tb^{3+}-doped samples. Representative emission spectra recorded from the samples subjected to annealing at different temperatures are shown in Fig. S5(a and b) of the ESI.† Emission from Eu^{3+} and Tb^{3+} was clearly observed for the as-prepared and 250 °C heated samples, while no emission was observed from samples heated above 350 °C. The excitation spectrum corresponding to the 615 nm emission from Eu^{3+} is shown in Fig. S6 of the ESI.† For the as-prepared and 250 °C heated samples, sharp intra-*4f* transitions of Eu^{3+} were superimposed over a broad background in the region of 280–450 nm in the excitation spectrum. The broad background peak was asymmetric and was likely arising due to the overlap of Eu–O charge transfer (320 nm) peak and the 6s → 6p inter-band transition (375 nm) of Bi^{3+} ions. The observation of the Bi^{3+} inter-band transition while monitoring Eu^{3+} emission confirmed the energy transfer from the host to Eu^{3+} ions. The results also confirmed the incorporation of Eu^{3+} into the host lattice for the as-prepared and 250 °C heated samples. In the case of high-temperature heated samples (temperatures above 350 °C), no distinct emission from Eu^{3+} species or host absorption could be observed, due to the phase segregation of lanthanide ions from the sillenite host.

Decay curves corresponding to the $^5D_0$ emission from all the Eu^{3+}-doped samples are shown in Fig. 5. All the decay

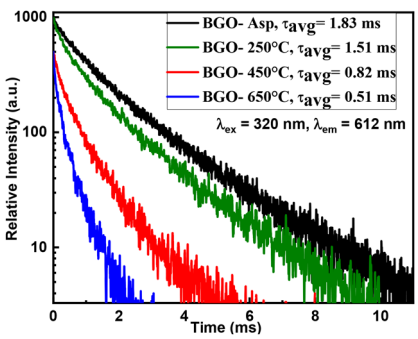

Fig. 5 Decay profiles corresponding to the $^5D_0$ level of Eu^{3+} in the as-prepared $Bi_{12}GaO_{20\pm\delta}$ (BGO-Asp) sample, along with those heated at various temperatures. Samples were excited at 320 nm, and emission was monitored at 612 nm.

curves were bi-exponential in nature, indicating varying local environments around the Eu^{3+} ions in the samples. Surface ions experienced different local environments compared to bulk ions, leading to distinct luminescence lifetimes.[34,35] The individual decay components for each sample, along with the respective chi-square values obtained after fitting, are provided in Table S2 of the ESI.† All the decay curves were characterised by a major long-lifetime component and a minor short-lifetime component. For the as-prepared and 250 °C heated samples, the long lifetime component was attributed to the Eu^{3+} ions present in the bulk, while the short lifetime component was attributed to Eu^{3+} ions present at the surface of nano-crystalline $Bi_{12}GaO_{20\pm\delta}$. For the samples heated at higher temperatures, namely 450 °C and 650 °C, multiple lifetime components arose due to phase segregation. From the lifetime components and their relative percentages, average values of the lifetime were evaluated and given in Table S2 of the ESI,† as well as indicated in the decay plot in Fig. 5. For the as-prepared sample, the average $^5D_0$ lifetime was found to be around 1.8 ms, with a marginal decrease in the lifetime value (~1.5 ms) for the 250 °C heated sample. For the samples heated at higher temperatures, namely 450 °C and 650 °C, the average lifetime value drastically decreased (around 50% or more), as shown in Fig. 5. In other words, Eu^{3+} luminescence underwent systematic quenching upon increasing the heat treatment temperatures. Low lifetimes and poor emission spectra confirmed the formation of a segregated Eu-rich phase for the samples heated above 350 °C, and XRD results further substantiated this. Peaks corresponding to the $Bi_{0.775}Eu_{0.225}O_{1.5}$ (ICSD code: 50641)[36] phase were clearly visible in the XRD pattern of the 650 °C heated samples (Fig. S7 of the ESI†).

At this point, it is worthwhile to understand why phase segregation of the lanthanide ion occurs from the sillenite host upon heating above 350 °C. To explore this, it is necessary to understand the type of network structure present in the bismuth gallate phase with sillenite structure. XRD patterns of the 450 °C and 650 °C heated samples were Rietveld refined, and the refined positional coordinates and lattice parameters were used to construct the polyhedra and the network structure in the sillenite host. This is depicted in Fig. 6. Five-coordinated distorted Bi^{3+} polyhedra with BiO_5LP (where LP represents the stereochemically active lone pair of electrons in the $6s^2$ orbital of Bi^{3+}) structural units edge-shared in the network. These edge-shared square pyramids corner-shared with GaO_4 tetrahedra to form a chain, and these chains formed the 3D network. The structural features mentioned above matched well with those reported earlier for such types of compounds.[37]

Computational studies

To understand the structure–property relationship, DFT calculations on $Bi_{24}Ga_2O_{40}$ with the *I*23 structure were carried out using VASP software. A single-point calculation was performed on the structure obtained through Rietveld refinement of the observed XRD pattern. The structure exhibited five different crystallographic sites: Bi1 (24f), Ga1 (2a), O1 (8c), O2 (24f) and O3 (8c). These sites were similar to those present in the conventional γ-Bi_2O_3 unit cell. Bi1 was surrounded by five oxygen atoms to form a distorted BiO_5E square pyramid, while Ga1 was coordinated by four O3 atoms leading to formation of GaO_4 tetrahedron. Fig. 7 shows the electron localization function (ELF) along the (020) plane of the unit cell. It is evident from the figure that ELF values were higher around the Bi atom. Previously,[37] it has been shown that the isosurface of a lobe-like charge distribution around the Bi atom is a signature of $6s^2$ LPEs. Thus, one can conjecture that the lone pairs are not exactly pointing toward the neighbouring Bi-atom; rather, they are tilted. The electronic structure of bismuth gallate is shown in Fig. 8. The valence band had a major contribution from the p-orbital of oxygen atoms, while the conduction band had dominant contributions from the p-orbitals of both Bi and oxygen atoms. The presence of Bi-6s states near the Fermi level in the valence band was considered a signature of stereochemically active lone pairs. In fact, the PDOS showed that the Bi-6s state was close to the valence band maximum for bismuth gallate.[38–40] The placement of the 6s state close to the valence band reduced the band gap. In fact, UV-visible optical absorption studies clearly showed a red shift in the wavelength corresponding to the onset of absorption (decrease in the optical gap) for the high-temperature heated samples (Fig. 2(a and b)). Hence, the experimental results were consistent with the inferences derived from theoretical studies.

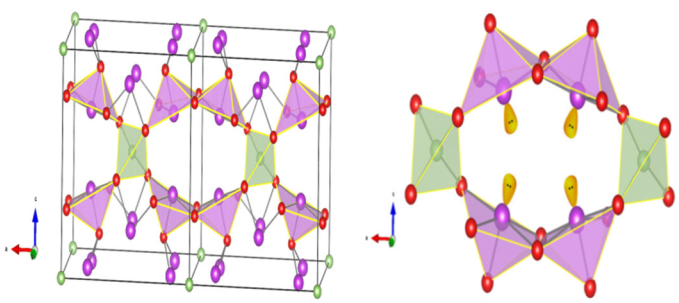

Fig. 6 (a and b) Schematic of the network structure. The $6s^2$ lone pairs of Bi^{3+} are shown in (b).

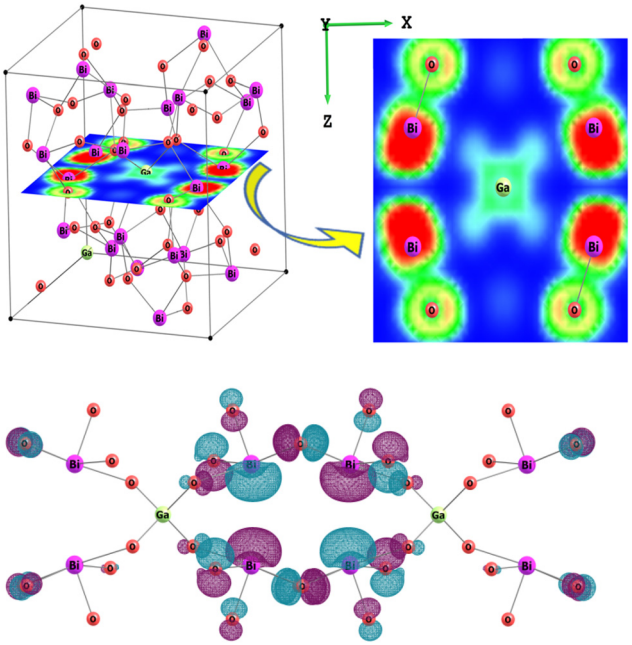

Fig. 7 (Top) Electron localization function (ELF) along the (020) plane for $Bi_{26}Ga_2O_{40}$ with the *I*23 space group. (Bottom) Molecular orbital diagram from cluster model calculations. In cluster model the hydrogen temination of terminal oxygens are not shown for clarity of presentation.

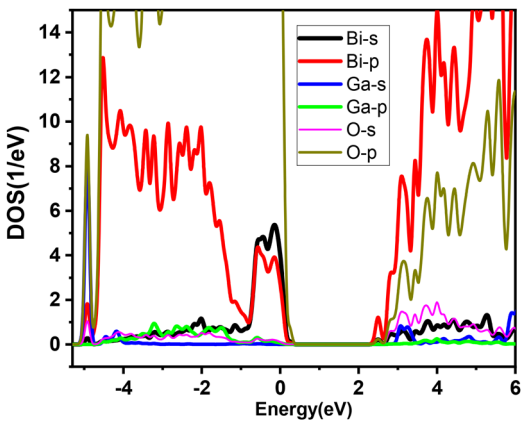

Fig. 8 Projected density of states for $Bi_{26}Ga_2O_{40}$ with the *I*23 space group.

In order to gain more insight at the orbital level, unrestricted Hartree–Fock (HF) calculations on a cluster model and the frontier molecular orbital having lone pair contributions are presented in Fig. 7 (bottom). It is observed that the molecular orbital with the lone pair contribution exhibited antibonding character. The phase of the wave function centered on the Bi atoms was opposite to that of the surrounding oxygen atoms. The antibonding character was a manifestation of the greater repulsive interaction between the two involved atoms (Bi and O). It is expected that in the nanostructure, owing to its finite size and large surface area, the average environment would deviate from square pyramidal symmetry.

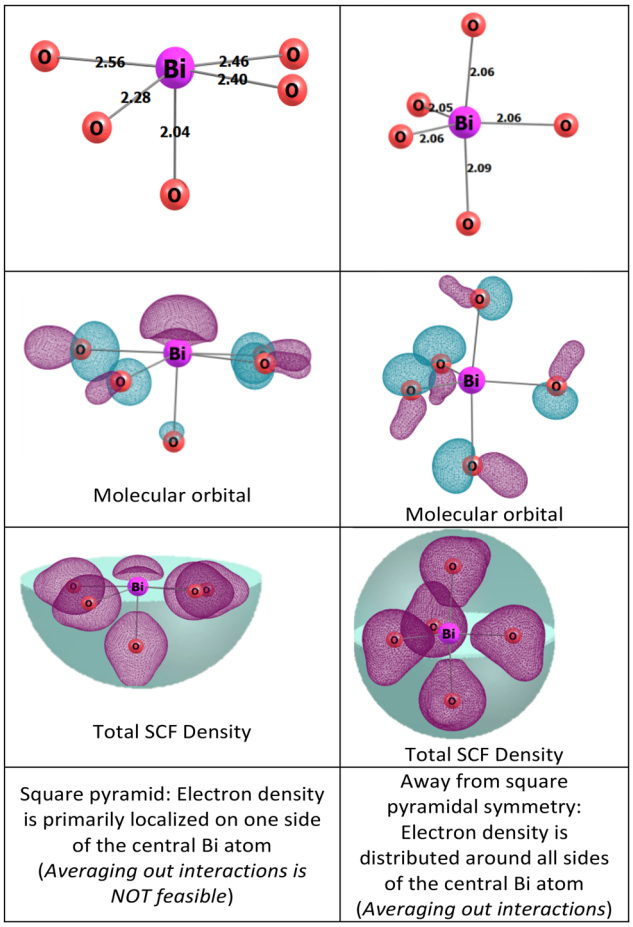

Fig. 9 HF calculations on the BiO_5 cluster model. In cluster model the hydrogen temination of terminal oxygens are not shown for clarity of presentation.

Based on this motif, unrestricted HF calculations on a BiO_5 cluster model (where terminal oxygens were terminated with hydrogen atoms) were carried out, and the results are presented in Fig. 9.

The optimization of the finite-sized BiO_5 led to a deviation from square pyramidal symmetry. Thus, it appeared quite obvious that nanocrystalline $Bi_{12}GaO_{20\pm\delta}$ would have BiO_5 units with a shift in square pyramidal symmetry. It is worth noting that in the square pyramidal BiO_5, the electron density was asymmetrically distributed, primarily on one side of the hemisphere, where averaging of interactions was not possible. Furthermore, in the square pyramidal BiO_5 unit, the lone pair electron density was also visible, similar to the $Bi_{12}GaO_{20\pm\delta}$ cluster model. However, the relaxed BiO_5 unit (structural unit with non-square pyramidal symmetry) had electron density in both hemispheres around the central Bi atom, leading to the averaging out of interactions. Interestingly, the relaxed BiO_5 (non-square pyramidal symmetry) units had closer Bi–O bonds, indicating a greater extent of bonding and resulting in the disappearance of the lone pair contribution.

Based on the above discussion, it is clear that bulk $Bi_{12}GaO_{20\pm\delta}$, having square pyramidal BiO_5 units, would have

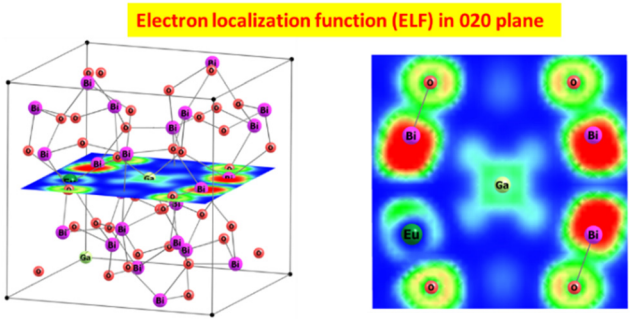

Fig. 10 ELF function of Eu^{3+}-substituted $Bi_{26}Ga_2O_{40}$ with the *I*23 space group.

stereochemically active lone pairs with asymmetrical electronic charge distribution, heavily biased towards one side of the hemisphere of the central Bi atom. In this biased electronic charge distribution, with antibonding-like features, the repulsive forces do not get averaged out locally. The long-range ordering due to the crystalline bulk nature resulted in the orientation of the lone pairs in a systematic fashion. In other words, there was a systematic balancing of repulsive interactions at each Bi site with a lone pair, translated crsytallographically (periodically translated according to crystallograpic symmetry). The inclusion of Eu or a rare earth ion disrupted this long-range balancing act, thereby destabilizing the system, as shown in Fig. 10.

Thus, the structure of $Bi_{12}GaO_{20\pm\delta}$ appeared to be a typical case of the balance of repulsive forces between the lone pair and the extent of long-range order among the lone pairs. The repulsion from the oxide ions pushed the lone pair in the (020) plane (since this plane was primarily occupied by bismuth atoms), and within the plane, the lone pairs did not point directly toward other facial bismuth atoms. Instead, they remained tilted to minimize the repulsion. As seen in Fig. 10, after the inclusion of europium (lanthanide) ions at the Bi site, the localized function disappeared at that site. Hence, the incorporation of lanthanide ions disrupted the balance between repulsive forces in the extended system, leading to phase instability.

In contrast, size-induced distortion in nanocrystalline $Bi_{12}GaO_{20\pm\delta}$ resulted in non-square pyramidal BiO_5E units, leading to a deviation from the biased electronic distribution to a more uniform distribution in both hemispheres around the central Bi atoms. This kind of uniform distribution (*in the context of spherical distribution of electronic charge*) led to the averaging out of interactions at local bismuth sites, resulting in a reduction in the stereochemical activity of the lone pair. Additionally, owing to the finite size, there would be no possibility of long-range translational repeatability of electronic effects. Hence, due to (i) the averaging out of interactions at local Bi sites and the associated suppression of stereochemical activity and (ii) the absence of long-range translational repeatability of electronic effects, the nanocrystalline sample would be able to accommodate the rare earth ion more comfortably compared to the bulk counterpart.

Perspectives

Based on the experimental and theoretical investigations described above, joint inferences were drawn and are presented as follows: one half of the BiO_5E square pyramid was bonded only to oxygen atoms, while the other half contained only $6s^2$ lone pair of electrons. This configuration applied to the samples heated at 450 °C and 650 °C, resulting in anisotropy in the electron cloud around Bi^{3+} for these samples. Although electronic anisotropy was present, long-range ordering of the lone pairs existed. Furthermore, the lone pairs were arranged in such a way that minimum repulsive forces existed between them. The regular arrangement of lone pairs with minimal repulsion led to the stereochemically active nature of the lone pair. Any disturbance in the long-range order, such as the incorporation of Ln^{3+} at the Bi^{3+} site, could result in drastic changes or imbalance in the repulsive forces between the lone pairs, leading to the collapse/destabilization of the network and the formation of lanthanide-rich bismuth oxides. This was, in fact, what occurred for the samples heated at 450 °C and 650 °C.

For the as-prepared, 250 °C and 350 °C heated samples, there existed a distribution in the bond angles and bond lengths around Bi^{3+}. The lone pairs attached to the Bi^{3+} species were oriented randomly within the network. Due to the distribution in bond angles and bond lengths, combined with the random orientation of lone pairs, the extent of spherical electronic anisotropy around Bi^{3+} was lesser in the as-prepared, 250 °C and 350 °C heated samples compared to that in the 450 °C and 650 °C heated samples. Thus, the lone pairs of the low-temperature heated samples were stereochemically inactive compared to those heated at 450 °C and 650 °C. Hence, for the low-temperature heated samples, the incorporation of Ln^{3+} at the Bi^{3+} site could not destabilize the structure, and hence lanthanide ions were retained within the structure. This was reflected in the luminescence properties of the Ln^{3+} ion discussed above. It is noteworthy that hosts such as $BiPO_4$ (both monoclinic and hexagonal forms) retain lanthanide ions substituted at the Bi^{3+} site in the host, even after heating at high temperatures.[23–25] However, in the case of $BiPO_4$, Bi^{3+} was coordinated with 8 or more oxygen atoms, allowing a uniform electron cloud to exist around Bi^{3+}. Thus, the lone pair did not play a significant role in determining the symmetry of the lattice/network and was considered stereochemically silent.

Conclusion

Crystalline sillenite-structured bismuth gallate with the composition $Bi_{12}GaO_{20\pm\delta}$ was prepared at low temperature using the polyol method, followed by heating at 450 °C. Based on detailed XRD, EDX and XRF techniques, it was confirmed that the synthesized sillenite phase was non-stoichiometric, with a composition of $Bi_{12}Bi_{0.19}Ga_{0.81}O_{19.5}$. The random orientation of lone pairs attached to Bi^{3+} ions, combined with its distributed local environment, led to stereochemically silent (inactive)

lone pairs in the low-temperature (as-prepared, 250 °C and 350 °C) heated samples. In contrast, for the high-temperature heated samples, the electronic distribution was quite anisotropic. This, combined with the long-range ordering of lone pairs, facilitated the creation of stereochemically active lone pairs. Detailed luminescence studies using lanthanide ions such as Er^{3+}, Eu^{3+} and Tb^{3+} as probe species established that the onset of stereochemical activity, along with the lack of balance between the repulsive forces, led to the loss (removal or attrition) of lanthanide ions from the lattice and phase segregation.

Author contributions

The synthesis, characterization, photoluminescence (PL) experiments, reproducibility checks and data plotting and tabulation were carried out by NS. The analysis of the results was conducted by VS, NS and SN. VS conceptualized the research idea and played a key role in reviewing and editing the manuscript at all stages. SN made significant contributions in rationalizing the results. SN performed the density functional theory (DFT) calculations, integrated the theoretical and experimental results and contributed significantly to the theoretical aspects of the manuscript. NG assisted with the X-ray photoelectron spectroscopy (XPS) measurements of the samples. CM contributed to the DFT calculations and analysis of the theoretical results. VS, SN and CM provided crucial feedback on the analysis and manuscript, assisting with its review and editing throughout the process. All authors have read, revised and approved the final version of the manuscript.

Data availability

The DFT calculations reported in the paper have been carried out using the Vienna *ab initio* simulation package (VASP) (**https://www.vasp.at/**). The cluster model Hartree–Fock (HF) calculations were carried out using GAMESS software (**https://www.msg.chem.iastate.edu/gamess/**).

The structural model used in the paper has been formulated using Vesta (**https://jp-minerals.org/vesta/en/**) and Chemcraft software (**https://www.chemcraftprog.com/**).

Conflicts of interest

The authors declare no competing financial interests.

Acknowledgements

We are grateful to the members of the Chemistry Division, BARC, for their kind cooperation during this work. We would also like to thank the SAIF Facility at IIT Bombay for providing the TEM images. NS thank HBNI, Mumbai for HBNI-DAE Senior Research Fellowship.

References

1 G. Laurita and R. Seshadri, A review of recent advances in material chemistry, *Acc. Chem. Res.*, 2022, **55**, 1004–1014.
2 O. Y. Khyzhun, V. S. Babizhetskyy, I. V. Kityk, G. L. Myronchuk, J. Jędryka, G. Lakshminarayana, V. O. Levytskyy, O. V. Tsisar, L. V. Piskach, O. V. Parasyuk, A. M. El Naggar, A. A. Albassam and M. Piasecki, Thallium indium germanium sulfide ($TlInGe_2S_6$) as efficient material for nonlinear optical applications, *J. Alloys Compd.*, 2018, **735**, 1694–1702.
3 A. Kojima, K. Teshima, Y. Shirai and T. Miyasaka, Organometal halide perovskites as visible-light sensitizers for photovoltaic cells, *J. Am. Chem. Soc.*, 2009, **131**, 6050–6051.
4 J. Lv, K. Dai, J. Zhang, L. Geng, C. Liang, Q. Liu, G. Zhu and C. Chen, Facile synthesis of Z-scheme graphitic-C_3N_4/Bi_2MoO_6 nanocomposite for enhanced visible photocatalytic properties, *Appl. Surf. Sci.*, 2015, **358**, 377–384.
5 Y. Feng, X. Yan, C. Liu, Y. Hong, L. Zhu, M. Zhou and W. Shi, Hydrothermal synthesis of CdS/Bi_2MoO_6 heterojunction photocatalysts with excellent visible-light-driven photocatalytic performance, *Appl. Surf. Sci.*, 2015, **353**, 87–94.
6 A. Walsh, D. J. Payne, R. G. Egdell and G. W. Watson, Stereochemistry of post-transition metal oxides: revision of the classical lone pair model, *Chem. Soc. Rev.*, 2011, **40**, 4455–4463.
7 M. Saura-Múzquiz, F. P. Marlton, B. G. Mullens, J. Liu, T. Vogt, H. E. Maynard-Casely, M. Avdeev, D. A. Blom and B. J. Kennedy, Cation and lone pair order–disorder in the polymorphic mixed metal bismuth scheelite $Bi_3FeMo_2O_{12}$, *Chem. Mater.*, 2023, **35**, 123–135.
8 A. Walsh and G. W. Watson, The origin of the stereochemically active Pb(II) lone pair: DFT calculations on PbO and PbS, *J. Solid State Chem.*, 2005, **178**, 1422–1428.
9 R. E. Brandt, V. Stevanović, D. S. Ginley and T. Buonassisi, Identifying defect-tolerant semiconductors with high minority-carrier lifetimes: beyond hybrid lead halide perovskites, *MRS Commun.*, 2015, **5**, 265–275.
10 A. Kudo, K. Omori and H. Kato, A novel aqueous process for preparation of crystal form-controlled and highly crystalline $BiVO_4$ powder from layered vanadates at room temperature and its photocatalytic and photophysical properties, *J. Am. Chem. Soc.*, 1999, **121**, 11459–11467.
11 A. Walsh, Y. Yan, M. N. Huda, M. M. Al-Jassim and S.-H. Wei, Band edge electronic structure of $BiVO_4$: elucidating the role of the Bi s and V d orbitals, *Chem. Mater.*, 2009, **21**, 547–551.
12 K. Ogawa, R. Abe and A. Walsh, Band gap narrowing by suppressed lone-pair activity of Bi^{3+}, *J. Am. Chem. Soc.*, 2024, **146**, 5806–5810.
13 S. K. Gupta, R. M. Kadam and P. K. Pujari, Lanthanide spectroscopy in probing structure–property correlation in multi-site photoluminescent phosphors, *Coord. Chem. Rev.*, 2020, **420**, 213405.

14 G. Blasse, Some considerations on rare-earth activated phosphors, *J. Lumin.*, 1970, **1–2**, 766–777.
15 G. Blasse and N. Sabbatini, The quenching of rare-earth ion luminescence in molecular and non-molecular solids, *Mater. Chem. Phys.*, 1987, **3–4**, 237–252.
16 G. Blasse, Chapter 34: Chemistry and Physics of R-Activated Phosphors, in *Handbook on the Physics and Chemistry of Rare Earths*, 1979, vol. 4, pp. 237–274.
17 S. Nigam, V. Sudarsan, C. Majumder and R. K. Vatsa, Structural Differences Existing in Bulk and Nanoparticles of $Y_2Sn_2O_7$: Investigated by Experimental and Theoretical Methods, *J. Solid State Chem.*, 2013, **200**, 202–208.
18 (*a*) S. Nigam, V. Sudarsan and R. K. Vatsa, Effect of Annealing Temperature on the Structural and Photoluminescence Properties of $Y_2Sn_2O_7$:Eu Nanoparticles, *Eur. J. Inorg. Chem.*, 2013, 357–363; (*b*) S. Nigam, V. Sudarsan and R. K. Vatsa, Improved luminescence from $Y_2Sn_2O_7$:Tb^{3+} nanoparticles co-doped with Sb^{3+} ions, *Opt. Mater.*, 2011, **33**, 558–562.
19 (*a*) D. K. Mal, S. Das, S. Nigam, B. P. Mandal, R. Kaiwart, H. K. Poswal, V. Sudarsan, C. Majumder and A. K. Tyagi, Revival of Stifled Luminescence in the $Y_2Sn_2O_7$:Eu Nano-Phosphor: Circumventing the Surface Side Effects by Zr–Eu Synergy, *New J. Chem.*, 2024, **48**, 17411–17422; (*b*) D. K. Mal, S. Das, S. Nigam, B. P. Mandal, R. Kaiwart, H. K. Poswal, V. Sudarsan, C. Majumder and A. K. Tyagi, Pyrochlore, like local structure in globally disordered Y2Zr2O7: Evidences and reasoning by combined theoretical and experimental study, *Inorg. Chem.*, 2024, **63**(49), 23248–23259.
20 A. Tyagi, S. Nigam, V. Sudarsan, C. Majumder, R. K. Vatsa and A. K. Tyagi, Why Do Relative Intensities of Charge Transfer and Intra-4f Transitions of Eu^{3+} Ion Invert in Yttrium Germanate Hosts? Unravelling the Underlying Intricacies from Experimental and Theoretical Investigations, *Inorg. Chem.*, 2020, **59**, 12659–12671.
21 J. Divya, N. J. Shivaramu, E. Coetsee, R. E. Kroon, W. Purcell and H. C. Swart, Enhanced Luminescence and Photocatalytic Activity of Bi_2O_3:Ho^{3+} Needles, *J. Alloys Compd.*, 2020, **842**, 155641.
22 M. Vila, C. Diaz-Guerra, K. Lorenz, J. Piqueras, E. Alves, S. Nappini and E. Magnano, Structural and Luminescence Properties of Eu and Er Implanted Bi_2O_3 Flowers for Optoelectronic Applications, *J. Mater. Chem. C*, 2013, **1**, 7920–7929.
23 M. Zhao, L. Li, J. Zheng, L. Yang and G. Li, Is $BiPO_4$ a Better Luminescent Host? Case Study on Doping and Annealing Effects, *Inorg. Chem.*, 2013, **52**, 807–815.
24 P. Arunkumar, C. Jayajothi, D. Jeyakumar and N. Lakshminarasimhan, Structure–Property Relations in Hexagonal and Monoclinic $BiPO_4$: Eu^{3+} Nanoparticles Synthesized by Polyol-Mediated Method, *RSC Adv.*, 2012, **2**, 1477–1485.
25 B. S. Naidu, B. Vishwanadh, V. Sudarsan and R. K. Vatsa, $BiPO_4$: A better host for doping lanthanide ions, *Dalton Trans.*, 2012, **41**, 3194–3203.
26 C. Zaldo, C. Coya, J. L. G. Fierro, K. Polgar, L. Kovács and Z. Szaller, X-Ray Photoelectron Spectroscopy and Optical Studies of $Bi_{12}(Ga_xBi_{1-x})O_{20-\delta}$ and $Bi_{12}(Zn_xBi_{1-x})O_{20-\delta}$ Single Crystals, *J. Phys. Chem. Solids*, 1996, **57**, 1667–1672.
27 K. D. Bomben, J. F. Moulder, P. E. Sobol and W. F. Stickle, *Handbook of X-Ray Photoelectron Spectroscopy: A Reference Book of Standard Spectra for Identification and Interpretation of XPS Data*, Physical Electronics, Eden Prairie, MN, USA, 1995.
28 D. Zheng, C. N. Young and W. F. Stickle, Hard X-ray photoelectron spectroscopy reference spectra of Bi with Cr Kα excitation, *Surf. Sci. Spectra*, 2023, **30**, 024024.
29 M. Valant and D. Suvorov, A Stoichiometric Model for Sillenites, *Chem. Mater.*, 2002, **14**, 3471–3476.
30 E. A. Davis and N. F. Mott, Conduction in Non-Crystalline Systems V. Conductivity, Optical Absorption, and Photoconductivity in Amorphous Semiconductors, *Philos. Mag.*, 1970, **22**, 903–922.
31 R. D. Shannon, Revised Effective Ionic Radii and Systematic Studies of Interatomic Distances in Halides and Chalcogenides, *Acta Crystallogr., Sect. A*, 1976, **32**, 751–767.
32 X. L. Chen, F. F. Zhang, Y. M. Shen, J. K. Liang, W. H. Tang and Q. Y. Tu, Phase Relations in the System $BiO_{1.5}$–$YbO_{1.5}$–CuO, *J. Solid State Chem.*, 1998, **139**, 398–403.
33 C. Lee, H. Park, W. Kim and S. Park, Origin of strong red emission in Er^{3+}-based upconversion materials: role of intermediate states and cross relaxation, *Phys. Chem. Chem. Phys.*, 2019, **21**, 24026.
34 V. Sudarsan, S. Sivakumar, F. C. J. M. van Veggel and M. Raudsepp, General and Convenient Method for Making Highly Luminescent Sol–Gel Derived Silica and Alumina Films by Using LaF_3 Nanoparticles Doped with Lanthanide Ions (Er^{3+}, Nd^{3+}, and Ho^{3+}), *Chem. Mater.*, 2005, **17**, 4736–4742.
35 J. W. Stouwdam and F. C. J. M. van Veggel, Near-infrared Emission of Redispersible Er^{3+}, Nd^{3+}, and Ho^{3+} Doped LaF_3 Nanoparticles, *Nano Lett.*, 2002, **2**, 733–737.
36 M. Drache, S. Obbade, J. P. Wignacourt and P. Conflant, Structural and Conductivity Properties of $Bi_{0.775}Ln_{0.225}O_{1.5}$ Oxide Conductors (Ln = La, Pr, Nd, Sm, Eu, Gd, Tb, Dy) with Rhombohedral Bi–Sr–O Type, *J. Solid State Chem.*, 1999, **142**, 349–359.
37 M. Weber, R. D. Rodriguez, D. R. T. Zahn and M. Mehring, γ-Bi_2O_3 - To Be or Not To Be? Comparison of the Sillenite γ-Bi_2O_3 and Isomorphous Sillenite-Type $Bi_{12}SiO_{20}$, *Inorg. Chem.*, 2018, **57**, 8540–8549.
38 K. Bu, H. Luo, S. Guo, M. Li, D. Wang, H. Dong, Y. Ding, W. Yang and X. Lü, Pressure-Regulated Dynamic Stereochemical Role of Lone-Pair Electrons in Layered Bi_2O_2S, *J. Phys. Chem. Lett.*, 2020, **11**, 9702–9707.
39 D. Wei, Y. Huang and H. J. Seo, Eu^{3+}-doped $Bi_7O_5F_{11}$ Microplates with Simultaneous Luminescence and Improved Photocatalysis, *APL Mater.*, 2020, **8**, 081109.
40 G. Agbeworvi, W. Zaheer, J. D. Ponis, J. V. Handy, J. R. Ayala, J. L. Andrews, P. Schofield, C. Jaye, C. Weiland, D. A. Fischer and S. Banerjee, Effect of Stereochemically Active Electron Lone Pairs on Magnetic Ordering in Trivanadates, *Inorg. Chem.*, 2023, **62**, 12965–12975.